Catalysis Letters (2020) 150:39–48
https://doi.org/10.1007/s10562-019-02947-9

Synthesis of $Sm_2MoO_6/Ni(OH)_2$ by Simple Impregnation Method: Photocatalyst for Non-precious Metal and Efficient Hydrogen Production

Zeying Liu[1] · Jing Xu[1,2,3] · Qiuting Liao[1] · Yanru Li[1] · Lingjiao Li[1] · Min Mao[1]

Received: 10 June 2019 / Accepted: 22 August 2019 / Published online: 9 September 2019

Abstract

$Sm_2MoO_6/Ni(OH)_2$ was successfully immersed in water first, and the sensitizer is Eosin Y and the sacrificial agent is triethanolamine agent for high-efficiency photocatalytic production of H_2. When Sm_2MoO_6 was loaded onto the surface of $Ni(OH)_2$, the photocatalytic activity (2407.48 μmol g^{-1} h^{-1}) was 2.6 times that of $Ni(OH)_2$ (925.36 μmol g^{-1} h^{-1}), which was Sm_2MoO_6 (169.36 μmol g^{-1} h^{-1}) is 14.2 times. From a series of characterizations, Sm_2MoO_6 is an effective cocatalyst to improve the separation of photo-generated charges and the efficiency of electron transfer. Large specific surface areas are a primary requirement for high efficiency catalysts, and the catalyst is sufficiently into contact with the sensitizer and the sacrificial agent to soar the photocatalytic activity.

Graphic Abstract

The first condition for an excellent catalyst is that it has a large specific surface area and can provide more active sites. In the dye sensitization system, the photocatalytic activity of $Sm_2MoO_6/Ni(OH)_2$ is 2.6 times that of $Ni(OH)_2$ and 14.2 times that of Sm_2MoO_6. Sm_2MoO_6 is an effective co-catalyst.

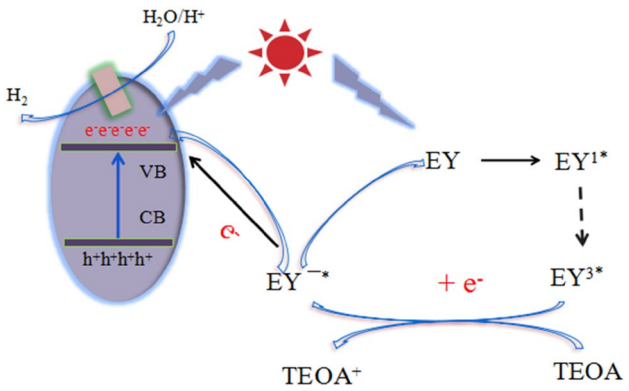

Keywords Sm_2MoO_6 · Photocatalytic · Rare earth

1 Introduction

Because traditional energy sources such as oil, coal, and natural gas are not renewable, they will destroy the atmosphere during use. Therefore, the energy issue has risen to social hotspots [1, 2]. Hydrogen is a renewable energy source that is non-polluting and can be obtained by water splitting [3–5]. The absorption range (ion doping, noble

✉ Jing Xu
wgyxj2000@163.com

Extended author information available on the last page of the article

metal loading, metal ion implantation, dye sensitization and conjugated polymer modification, etc.) can be expanded by modification, and a novel oxide photocatalyst having visible light-driven activity can be developed to improve sunlight utilization [6–8]. At present, obtaining efficient, stable and inexpensive photocatalytic water-decomposing photocatalysts remains a huge challenge [9].

Ni-based materials are effective catalysts for such energy conversion and storage reactions as the oxygen evolution, the oxygen reduction and supercapacitors [10–12]. Because nano-$Ni(OH)_2$ has good electrochemical performance, proton diffusion coefficient, fast activation speed and grain resistance are low, it has become a hot topic in the research fields of optoelectronic materials, gas sensing materials and battery cathode materials [13, 14]. As a hydrolysis accelerator, $Ni(OH)_2$ can destroy the H–OH bond after introduction, thereby increasing the catalytic activity [15]. $Ni(OH)_2$ can be prepared by precipitation [16], hydrothermal synthesis [17], and ion exchange [18]. When the mass ratio of the flower $Ni/Ni(OH)_2$ to CdS is 0.5, the hydrogen production rate is 373.5 μmol h^{-1}, which is 1.7 times that of 1 wt% Pt/CdS [19].

Rare earth compound based on an electronic, optical and chemical properties of the 4f electron generation, are widely used in high-performance light emitting device, the catalyst material and other functional areas [20, 21]. Metal molybdate is a typical binary metal oxides having abundant resources and non-toxic [22–24]. Transition metal molybdate can be used for photochemical degradation of different dyes [25–27]. It is reported that the samarium molybdic can be used as a fluorescent agent, and the preparation method is complicated [21, 28]. However, there have been few studies using rare earth molybdate as a photocatalyst. We used a simple method to prepare rare earth molybdate (mixing $(NH_4)_6Mo_7O_{24}{\cdot}4H_2O$ and $Sm(NO_3)_3{\cdot}6H_2O$ at a molar ratio of 1:1 at ambient temperature) for the first time as a cocatalyst. The photocatalytic activity of $Ni(OH)_2$ is effectively improved. $Sm_2MoO_6/Ni(OH)_2$ was successfully prepared by simply hydrothermal then impregnation. $Sm_2MoO_6/Ni(OH)_2$ composites has strong photocatalytic activity and high photocatalytic stability under visible light irradiation.

2 Experimental Section

2.1 Preparation of Catalysis

Synthesis of $Ni(OH)_2$ nanosheets: Added 900 mg urea and 1087.6 mg $Ni(NO_3)_2{\cdot}6H_2O$ to 60 mL of ethylene glycol solution (25 mL water and 57.5 mL ethylene glycol). Stirred for 1 h and heat at 120 °C for 4 h. The product was collected by centrifugation and washed several times with water and ethanol.

Synthesis of Sm_2MoO_6: Added $(NH_4)_6Mo_7O_{24}{\cdot}4H_2O$ and $Sm(NO_3)_3{\cdot}6H_2O$ to 60 mL of deionized water. After stirred for 12 h, the product was collected and washed several times with water and ethanol. The molar ratio of $(NH_4)_6Mo_7O_{24}{\cdot}4H_2O$ to $Sm(NO_3)_3{\cdot}6H_2O$ was 1:1.

Synthesis of $Sm_2MoO_6/Ni(OH)_2$: Dispersed 100 mg of $Ni(OH)_2$ nanosheet into 60 mL of deionized water solution. Added a certain amount of $(NH_4)_6Mo_7O_{24}{\cdot}4H_2O$ and $Sm(NO_3)_3{\cdot}6H_2O$ (the molar ratio of $(NH_4)_6Mo_7O_{24}{\cdot}4H_2O$ and $Sm(NO_3)_3{\cdot}6H_2O$ is 1:1.). After stirred for 12 h, the product was collected and washed several times with water and ethanol.

All of the above catalysts were dried at 60 °C for 4 h.

2.2 Characterizations

The morphology of the sample was measured by TEM and HRTEM (HRTEM, JEOL JEM-2100, Japan). The chemical structure of the sample is determined by X-ray diffraction (XRD, Rigaku RINT-2000), and CuKα was irradiated at 30 mA and 40 kV. The chemical elements were determined by X-ray photoelectron spectroscopy (XPS, ESCALAB 250Xi). Fluorescence spectra were determined by a FluoroMAX-4 spectrometer (HORIBA Scientific, France). The specific surface area was measured by a Micromeritics ASAP 2020 nitrogen adsorption unit.

2.3 Photocatalytic Hydrogen Production

The photocatalytic hydrogen production experiment was carried out in a 250 mL closed quartz bottle, and the light source was a 300 W Xe lamp ($\lambda \geq 420$ nm). The 20 mg photocatalyst was added to 100 mL TEOA (10%) solution. After ultrasonic dispersion for 10 min, 50 mg of Eosin Y were added, and the dark gas was stirred magnetically for 30 min, and nitrogen was purged for 40 min. The 0.5 mL of H_2 was extracted every 1 h under visible light, and the generated hydrogen was measured by gas chromatography (N_2 as a carrier gas) using a 13X molecular sieve column and a thermal conductivity detector (TCD).

2.4 Photoelectrochemical Measurements

Photocurrent measurements were performed on an electrochemical workstation (CHI660D, CH Instruments, China) with an electrolyte solution of 0.1 M Na_2SO_4. The catalyst was ultrasonically dispersed in absolute ethanol for 30 min to prepare a slurry, which was applied onto the surface of an ITO conductive glass and dried at room temperature to obtain a working electrode having an effective area of 1×1 cm^2. The light source is a 300 W Xe lamp ($\lambda \geq 420$ nm). The prepared sample electrode was used as the working electrode, the platinum wire was the counter electrode and the

standard, and the saturated calomel electrode (SCE) was used as the reference electrode.

3 Results and Discussion

3.1 XRD

Figure 1 is the XRD pattern of $Ni(OH)_2$, Sm_2MoO_6 and $Sm_2MoO_6/Ni(OH)_2$. The 2θ of Sm_2MoO_6 is 28.10° and 47.28°, which corresponding to the (− 321) and (640) crystal planes of Sm_2MoO_6, respectively. The crystal face is identical the monoclinic phase of Sm_2MoO_6 (PDF-#24-0997). The 2θ of $Ni(OH)_2$ is 11.63°, 22.56°, 33.67°, 37.48° and 59.60°, corresponding to (001), (002), (110), (200) and (300) of $Ni(OH)_2$, respectively. The crystal face is identical to the hexagonal phase $Ni(OH)_2$ (PDF-#22-0444). The diffraction peak of $Sm_2MoO_6/Ni(OH)_2$ is consistent with $Ni(OH)_2$ and Sm_2MoO_6. It is indicated that $Ni(OH)_2$, Sm_2MoO_6 and $Sm_2MoO_6/Ni(OH)_2$ are successfully prepared. The particle size of the sample can be calculated according to the Scherrer formula. The crystallite size of $Ni(OH)_2$ is 13.60–68.47 nm, the crystallite size of Sm_2MoO_6 is 37.71–47.19 nm, and the crystallite size of $Sm_2MoO_6/Ni(OH)_2$ is 14.71–73.02 nm. The results show that the composite catalyst $Sm_2MoO_6/Ni(OH)_2$ with rare earth molybdate as cocatalyst was successfully prepared.

3.2 XPS

The elemental composition and valence state analysis of the composite photocatalyst $Sm_2MoO_6/Ni(OH)_2$ was provided by X-ray photoelectron spectroscopy (XPS). Figure 2a is the total spectrum of $Sm_2MoO_6/Ni(OH)_2$, which indicates the presence of Sm, Mo, Ni and O elements in the composite catalyst. Figure 2b is the XPS of Ni 2p with two strong peaks of 855.2 eV and 872.8 eV corresponding to $Ni2p_{3/2}$ and Ni $2p_{1/2}$, respectively. This is the classical value of Ni^{2+} in $Ni(OH)_2$. Two satellite peaks were also observed with binding energies of 861.0 eV and 879.5 eV [29]. Figure 2c is the XPS of Sm 3d, the two peaks with binding energies of 1083.5 eV and 1110.4 eV are Sm $3d_{5/2}$ and Sm $3d_{3/2}$, respectively. It is indicated that Sm exists in the form of Sm^{3+} in Sm_2MoO_6 [30]. Figure 2d is the XPS of Mo 3d. The two peaks with binding energies of 235.0 eV and 232.0 eV correspond to Mo $3d_{3/2}$ and Mo $3d_{5/2}$, respectively. The difference between the two peaks is 3 eV. It is indicated that Mo exists in the form of Mo^{6+} in Sm_2MoO_6 [31]. Figure 2e is the XPS of O 1 s, and the peak with a binding energy of 531.0 eV is attributed to Sm_2MoO_6.

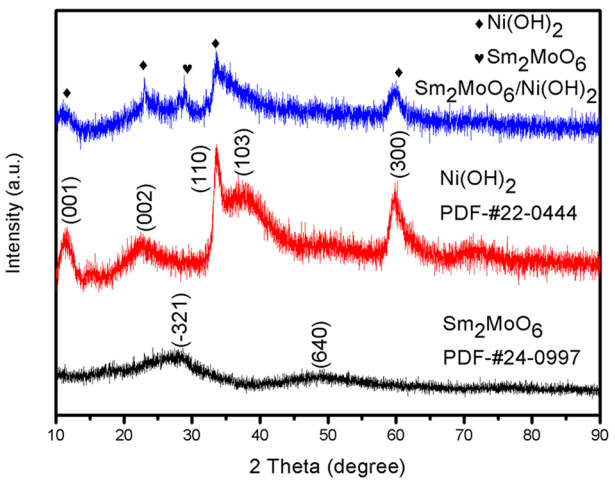

Fig. 1 XRD patterns of the as-prepared $Ni(OH)_2$, Sm_2MoO_6 and $Sm_2MoO_6/Ni(OH)_2$

3.3 TEM

Figure 3a is a TEM of 3% $Sm_2MoO_6/Ni(OH)_2$, and the catalyst consists of nanosheets in the form of fungus. Figure 3b is the HRTEM of 3% $Sm_2MoO_6/Ni(OH)_2$ with a lattice spacing of 0.76 nm corresponding to the (001) crystal plane of $Ni(OH)_2$. The lattice spacing is 0.31 nm, which corresponds to the (− 321) crystal plane of Sm_2MoM_6. It is in keeping with the XRD results. Figure 3d–g is the STEM image of 3% $Sm_2MoO_6/Ni(OH)_2$ and corresponding energy dispersive X-ray (EDX) element mapping images of Ni, Mo, Sm and O, indicating that all elements are present in photocatalyst, and evenly distributed.

3.4 BET

The large specific surface area provides more active sites and can adsorb more EY. Figure 4a is the N_2 adsorption–desorption isotherm of Sm_2MoO_6, $Ni(OH)_2$ and 3% $Sm_2MoO_6/Ni(OH)_2$. $Sm_2MoO_6/Ni(OH)_2$ and $Ni(OH)_2$ have a type III isotherm. Sm_2MoO_6 and $Sm_2MoO_6/Ni(OH)_2$ have an H3 hysteresis loop and are slit holes formed by stacking of flaky particles. $Ni(OH)_2$ has an H4 hysteresis loop and is a slit hole produced by a layered structure. Figure 4b shows the pore size distribution curve. Sm_2MoO_6, $Ni(OH)_2$ and 3% $Sm_2MoO_6/Ni(OH)_2$ have a similar curve, mainly 0–50 nm mesopores. Table 1 is the specific surface area, pore size and pore volume of the catalyst. The specific surface area of $Ni(OH)_2$ is 78.78 $m^2\ g^{-1}$. After loading Sm_2MoO_6, the specific surface area was 148.55 $m^2\ g^{-1}$. As is clear from Table 1, the specific surface area and pore volume of $Sm_2MoO_6/Ni(OH)_2$ are the largest. This is due to the growth of Sm_2MoO_6 on the surface of $Ni(OH)_2$. The high specific surface area and large pore volume of the composite are beneficial for the decomposition of hydrogen produced by hydrogen in photocatalytic applications.

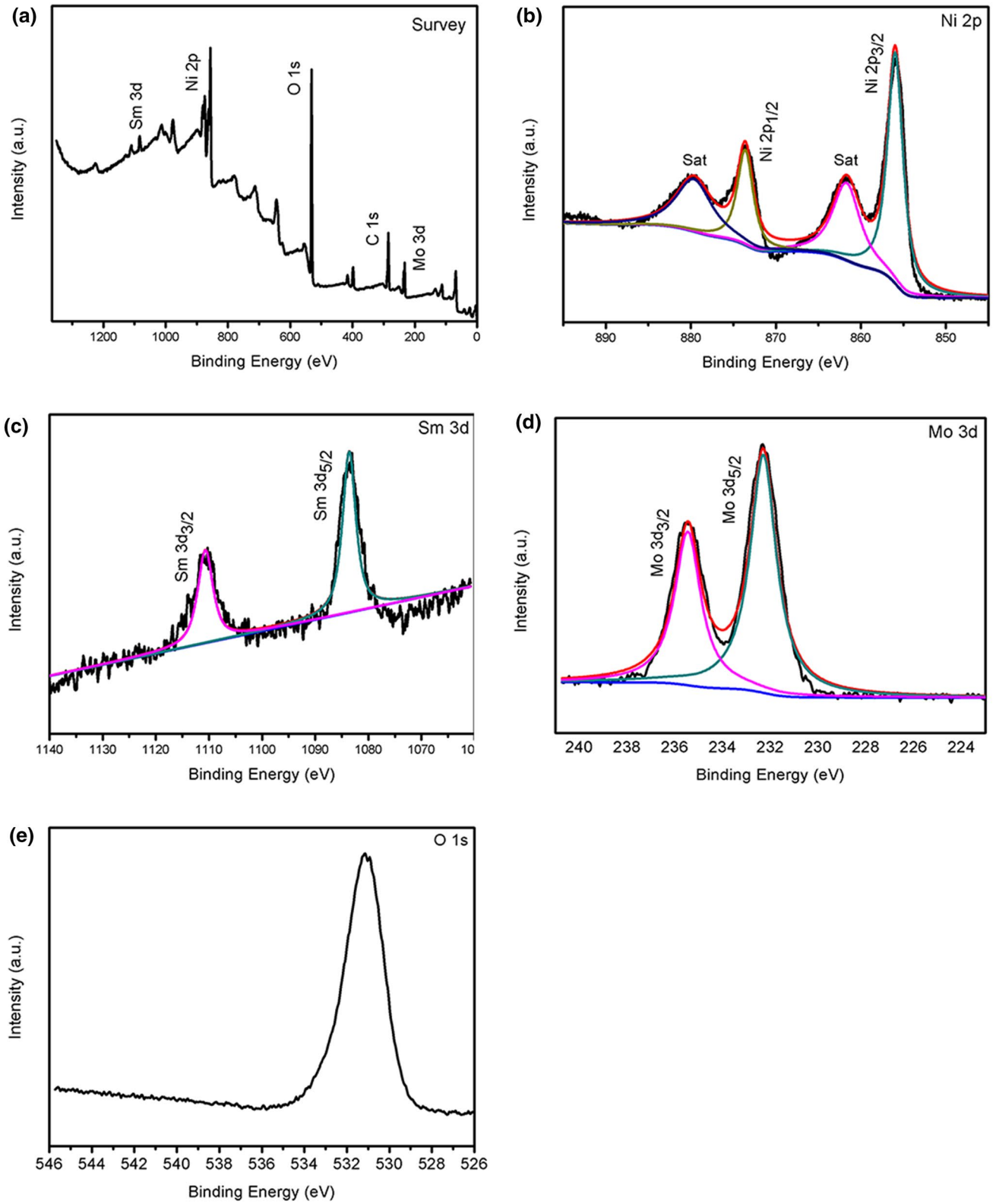

Fig. 2 XPS spectra of $Sm_2MoO_6/Ni(OH)_2$ samples: **a** survey spectra; **b** Ni 2p; **c** Sm 3d; **d** Mo 3d; **e** O 1s

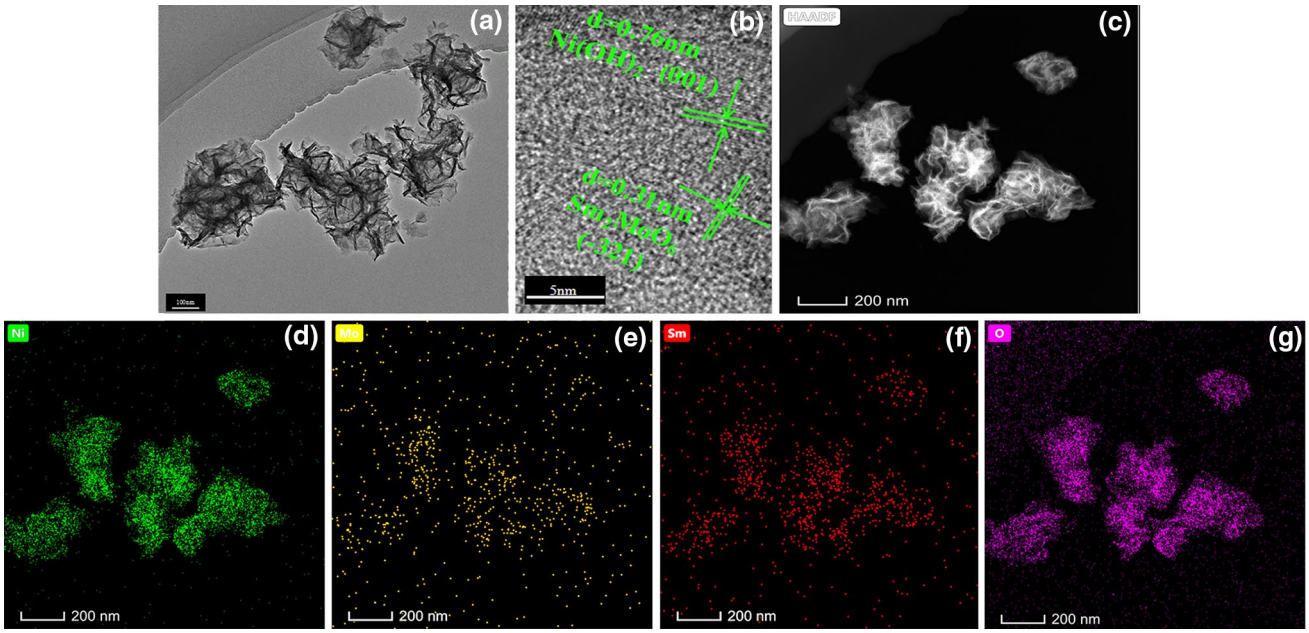

Fig. 3 TEM (**a**) and HRTEM (**b**) images of $Sm_2MoO_6/Ni(OH)_2$; STEM image (**c**) and EDX elemental mapping of Ni (**d**), Mo (**e**), Sm (**f**) and O (**g**)

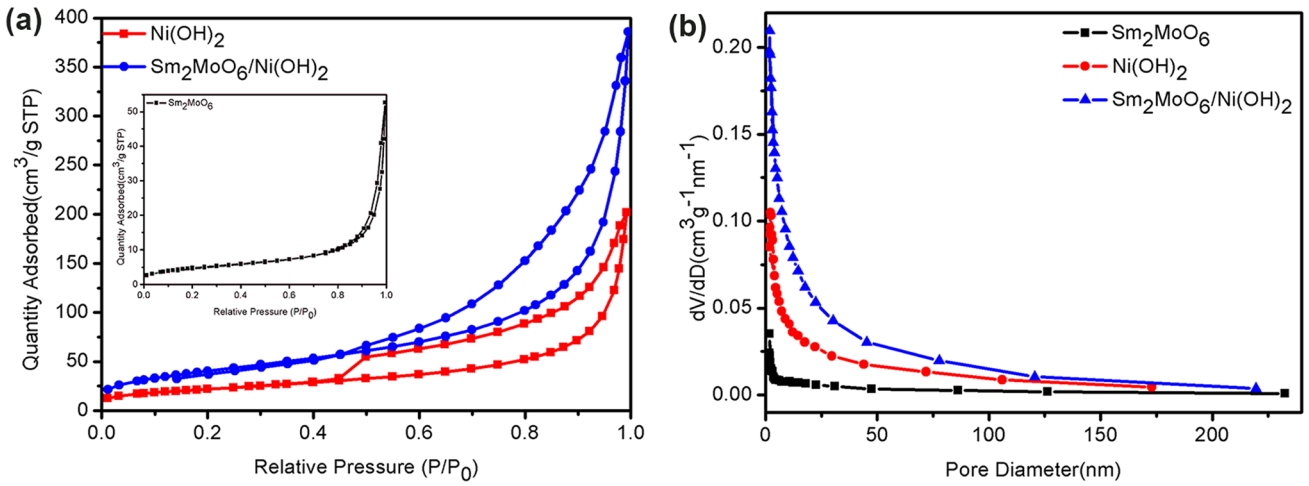

Fig. 4 **a** The N_2 adsorption–desorption isotherms of Sm_2MoO_6, $Ni(OH)_2$ and 3% $Sm_2MoO_6/Ni(OH)_2$; **b**The pore size distributioncurves of Sm_2MoO_6, $Ni(OH)_2$ and 3% $Sm_2MoO_6/Ni(OH)_2$

Table 1 The S_{BET}, pore volume for Sm_2MoO_6, $Ni(OH)_2$ and 3% $Sm_2MoO_6/Ni(OH)_2$

Samples	S_{BET} (m^2g^{-1})	Pore size (nm)	Pore volume (cm^3g^{-1})
Sm_2MoO_6	17.17	18.98	0.08
$Ni(OH)_2$	78.78	15.83	0.31
$Sm_2MoO_6/Ni(OH)_2$	148.55	16.07	0.60

3.5 Photocatalytic Hydrogen Evolution

Figure 5a is the photocatalytic hydrogen production activity of $Ni(OH)_2$, Sm_2MoO_6 and 3% $Sm_2MoO_6/Ni(OH)_2$ was tested by using triethanolamine as a sacrificial agent and Eosin Y as a sensitizer. Among them, the hydrogen production of Sm_2MoO_6 at 5 h is 42.34 μmol. The hydrogen production of $Ni(OH)_2$ at 5 h is 231.34 μmol. The hydrogen

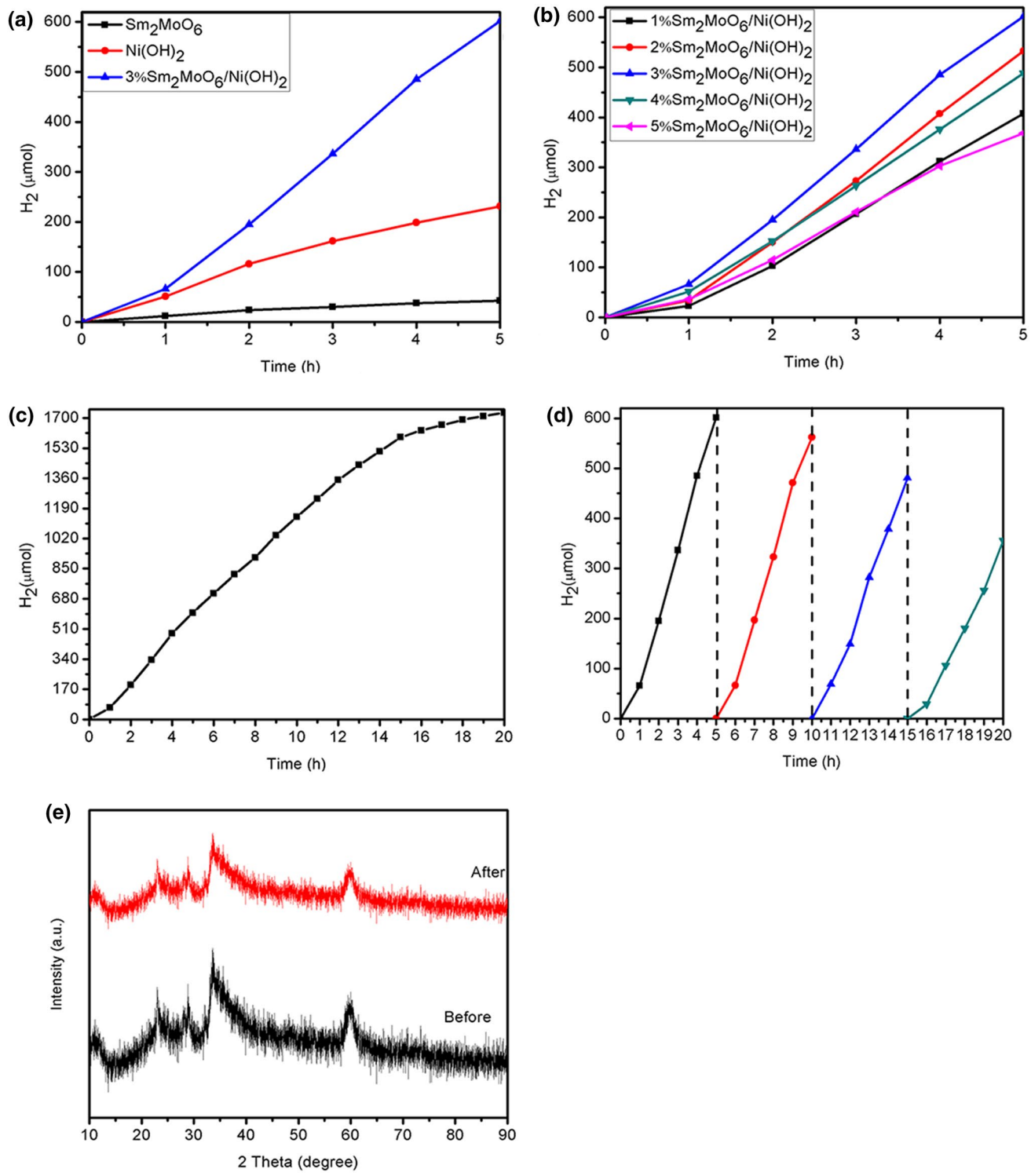

Fig. 5 **a** Photocatalytic activities of different catalysts; **b** photocatalytic activity of $Sm_2MoO_6/Ni(OH)_2$ with different molar ratios; **c** photocatalytic activity of $Sm_2MoO_6/Ni(OH)_2$ for 20 h of continuous illumination; **d** stability of photocatalytic activity of 3% $Sm_2MoO_6/Ni(OH)_2$; **e** XRD pattern of 3% $Sm_2MoO_6/Ni(OH)_2$ before and after 4 hydrogen production cycles

production of 3% $Sm_2MoO_6/Ni(OH)_2$ at 5 h is 601.87 μmol, which is 14.2 times that of Sm_2MoO_6 and 2.6 times that of $Ni(OH)_2$. The photocatalytic performance is significantly improved. Sm_2MoO_6 can be used as a high-efficiency cocatalyst to significantly improve the separation efficiency of electron photogenerated electron–holes and accelerate the

electron transfer on the surface of the composite photocatalyst to promote hydrogen evolution activity.

Figure 5b shows that when the content of $Ni(OH)_2$ is constant, the content of Sm_2MoO_6 is the key to the optimum photocatalytic activity, and the loading of Sm_2MoO_6 is from 1 to 5%. The introduction of Sm_2MoO_6 concentration from 1 to 3% onto $Ni(OH)_2$ can gradually enhance the photocatalytic hydrogen production activity by promoting charge collection. When the loading of Sm_2MoO_6 reaches 3%, $Sm_2MoO_6/Ni(OH)_2$ exhibits the best photocatalytic activity. However, when the loading amount of Sm_2MoO_6 exceeds 3%, the photocatalytic activity is remarkably lowered. This is because the excess Sm_2MoO_6: (1) covers the active site on the surface of $Ni(OH)_2$, hindering its contact with the sacrificial agent and the sensitizer; (2) shielding the incident light and preventing the generation of light absorption and photogenerated charge; (3) as a charge recombination center. Therefore, the optimum loading of Sm_2MoO_6 for optimal hydrogen production is 3%.

In order to evaluate the stability of $3\%Sm_2MoO_6/Ni(OH)_2$, we measured several cycles and the photocatalytic activity of continuous light for 20 h changed with time. Figure 5c shows the amount of hydrogen produced by continuous irradiation for 20 h. During the 20 h of illumination, the hydrogen production of $3\%Sm_2MoO_6/Ni(OH)_2$ reached 1733.32 μmol, indicating a stable photocatalytic activity of about 4333.3 $\mu mol \cdot g^{-1} \cdot h^{-1}$. And after the 15th h, the amount of hydrogen production increased slowly due to the reduction of the sensitizer and the sacrificial agent.

As shown in Fig. 5d, during the four cycles with a total reaction time of 20 h, the first three photocatalytic activities were relatively stable. There was a significant decrease in the fourth cycle, which was due to the reduction of sensitizer and sacrificial agent in the reaction system, indicating that $Sm_2MoO_6/Ni(OH)_2$ has good photocatalytic hydrogen production stability.

Figure 5e is the XRD of the catalyst before and after illumination. XRD before and after illumination showed a decrease in diffraction peaks, but there was no significant change. The results show that the photocatalytic activity of the catalyst is relatively stable.

3.6 PL Analysis

Figure 6 is a steady-state fluorescence spectrum of EY, Sm_2MoO_6, $Ni(OH)_2$ and $Sm_2MoO_6/Ni(OH)_2$. Generally, the level of electron–hole recombination can be judged by the level of fluorescence intensity. The maximum emission peak position of EY is 538 nm. The PL emission peak of Sm_2MoO_6 was observed at a wavelength of 540 nm, and the fluorescence intensity was lowered. The fluorescence intensity of $Ni(OH)_2$ also decreased, and the fluorescence intensity of $Sm_2MoO_6/Ni(OH)_2$ was the lowest. It is indicated that after the modification of $Ni(OH)_2$ by Sm_2MoO_6, the electron–hole separation rate is improved and the photocatalytic activity is improved. It is indicated that Sm_2MoO_6 facilitates the separation of electron-holes and improves the electron transfer efficiency, thereby promoting photocatalytic activity. Prove that Sm_2MoO_6 is a highly efficient cocatalyst.

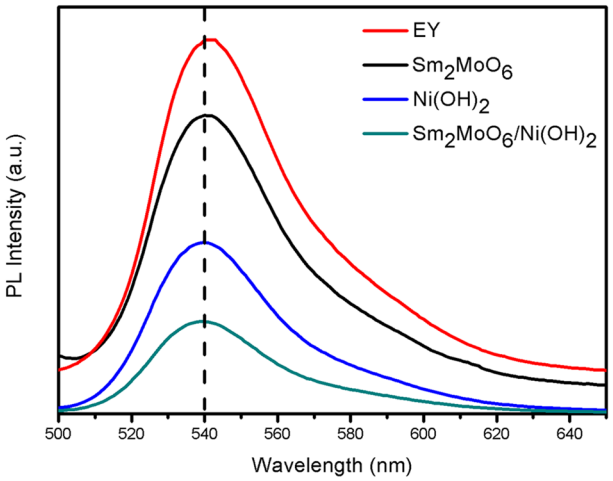

Fig. 6 PL spectra of EY, Sm_2MoO_6, $Ni(OH)_2$ and $Sm_2MoO_6/Ni(OH)_2$ samples

3.7 Electrochemical Analysis

In order to find out the mechanism for enhancing the photocatalytic hydrogen production activity of $Sm_2MoO_6/Ni(OH)_2$, a series of experiments were conducted. As shown in Fig. 7a, we first measure the transient photocurrent response of the sample. The photocatalyst can generate electron-hole pairs under the light, oxidize electrons on the Pt electrode, and reduce holes on the working electrode. There is a transient photocurrent response curve at four intermittent illuminations, and there is a fast and uniform photocurrent response with light illumination on and off, indicating that all samples can be used as excellent photocatalysts. The transient photocurrent response of $Sm_2MoO_6/Ni(OH)_2$ is much larger than the transient photocurrent response of Sm_2MoO_6 and $Ni(OH)_2$. The results show that the separation efficiency of photogenerated carriers in $Sm_2MoO_6/Ni(OH)_2$ is high, which indicates that Sm_2MoO_6 can effectively improve the photoinduced charge separation and the transfer efficiency, thereby improving the photocatalytic activity.

We show the catalytic HER activity of $Sm_2MoO_6/Ni(OH)_2$. For comparison, similar electrochemical measurements of Sm_2MoO_6 and $Ni(OH)_2$ were also performed. Figure 7b shows the LSV curve with a scan rate of 0.5 mV s^{-1}. Compared with Sm_2MoO_6 and $Ni(OH)_2$, $Sm_2MoO_6/Ni(OH)_2$

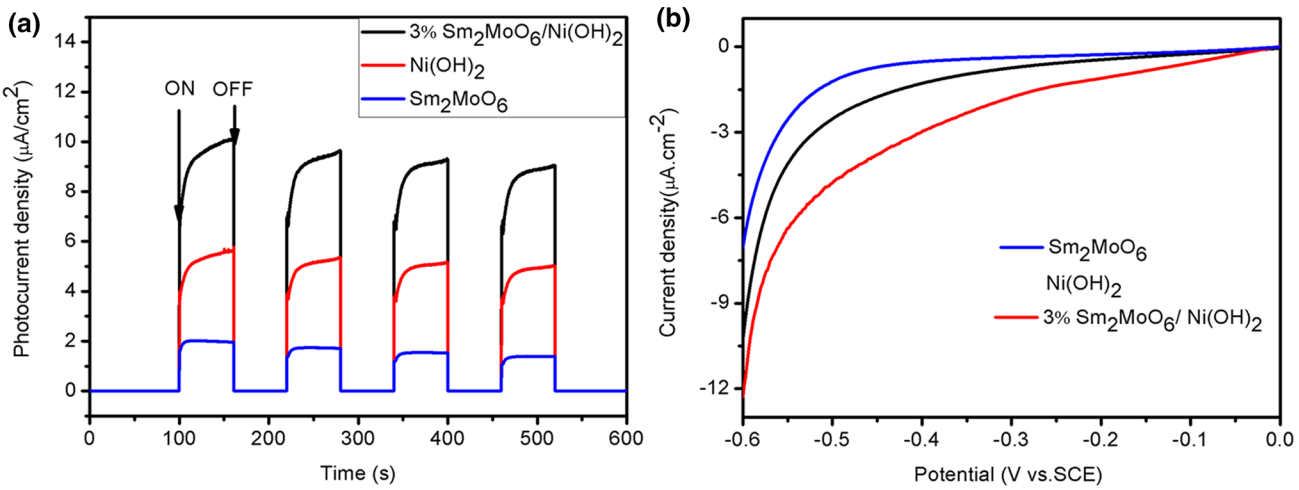

Fig. 7 **a** Transient photocurrent responses; **b** LSV curses of photo-catalytic in Na_2SO_4 (0.2 mol/L). The scan rate was 0.5 mV s^{-1}

has the lowest overpotential. Because photocatalytic hydrogen production depends on the overpotential of the HER reaction, the results clearly indicate that $Sm_2MoO_6/Ni(OH)_2$ is a better photocatalyst.

3.8 Photo-Catalytic Mechanism

Based on the above results, a possible photocatalytic hydrogen production mechanism is proposed in Fig. 8. Both the EY molecule and $Ni(OH)_2$ can be photoexcited under the irradiation of visible light. Electron transfer and reaction are mainly divided into the following two parts: (1) The EY molecule absorbs photons to form a single excited state EY^{1*}, and EY^{1*} forms a triplet excited state through intersystem transitions. $EY^{3}*$ is reduced by TEOA to produce $EY^{-\cdot}$ and oxidized electron donors. $EY^{-\cdot}$ is transferred to $Ni(OH)_2$ and further transferred to the reaction site of Sm_2MoO_6. Protons are reduced by electrons to produce H_2. (2) $Ni(OH)_2$ absorbs photons to generate electrons and holes, and electrons are transferred to the conduction band while the holes remain in the valence band. Electrons are transferred to Sm_2MoO_6, reducing protons to produce H_2, and holes are reduced by TEOA. The EY molecule is returned to the ground state. Due to the synergy between $Ni(OH)_2$ and Sm_2MoO_6, the charge transfer rate is promoted and the photocatalytic activity is improved. The corresponding chemical reaction is as follows:

$$\begin{cases} EY \xrightarrow{hv} EY^{1*} \xrightarrow{ISC} EY^{3*} EY^{3*} + TEOA \rightarrow EY^{-} + TEOA^{+} \\ EY^{-\cdot}(e^{-}) \rightarrow Ni(OH)_2(e^{-}_{CB}) \rightarrow Sm_2MoO_6(e^{-}_{CB}) \\ 2e^{-} + 2H_2O \rightarrow H_2 + 2OH^{-} \\ h^{+} + TEOA \rightarrow TEOA^{+} \end{cases}$$

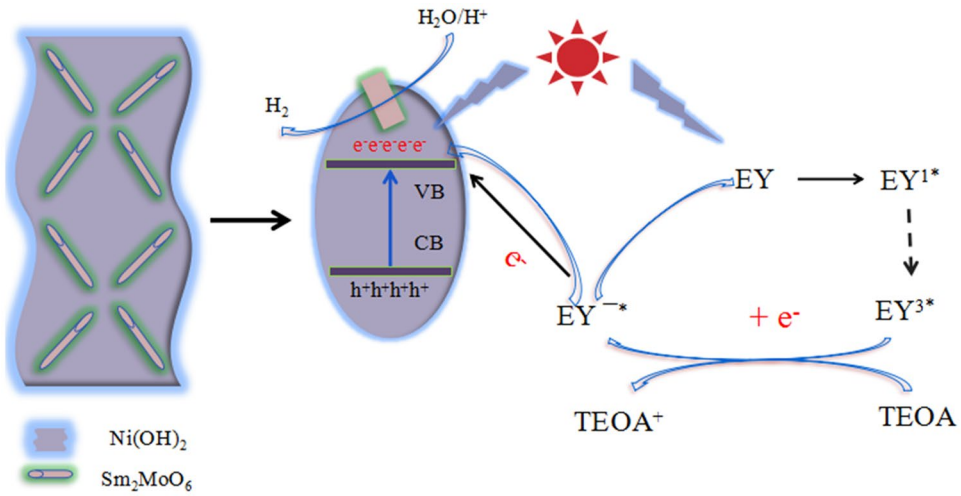

Fig. 8 The photocatalytic hydrogen production mechanism over EY sensitized $Sm_2MoO_6/Ni(OH)_2$ system under visible light irradiation

$$\begin{cases} Ni(OH)_2 \xrightarrow{h\nu} e^-_{CB} + h^+_{VB} \\ 2e^- + 2H_2O \rightarrow H_2 + 2OH^- \\ h^+ + TEOA \rightarrow TEOA^+ \end{cases}$$

4 Conclusions

For the first time, using Sm_2MoO_6 as a cocatalyst, the photocatalytic activity of $Ni(OH)_2$ was significantly improved. Sm_2MoO_6/$Ni(OH)_2$ was prepared by first hydrothermal followed by impregnation. Sm_2MoO_6/$Ni(OH)_2$ has a high specific surface area, which is a major requirement for an effective catalyst, providing more active sites and allowing the catalyst to be in sufficient contact with the sensitizer and the sacrificial agent. From photocurrent response and steady-state fluorescence, Sm_2MoO_6 can effectively improve the electron transfer efficiency of Sm_2MoO_6/$Ni(OH)_2$ and inhibit the recombination of electrons and holes. The hydrogen production rate of 3% Sm_2MoO_6/$Ni(OH)_2$ was 2407.48 μmol g^{-1} h^{-1}, which was 14.2 times that of Sm_2MoO_6 and 2.6 times that of $Ni(OH)_2$. Moreover, the stability of 3% Sm_2MoO_6/$Ni(OH)_2$ is good. Due to the synergistic effect between Sm_2MoO_6 and $Ni(OH)_2$, the rapid transfer of charge can be promoted and the efficiency and activity of photocatalytic hydrogen production can be improved. Sm_2MoO_6 is a potentially efficient cocatalyst.

Acknowledgements This work was supported by the Natural Science Foundation of Ningxia Province (NZ17262).

Compliance with Ethical Standards

Conflict of interest There are no conflicts to declare.

References

1. Zhang J, Liu Y, Xia B et al (2018) Facile one-step synthesis of phosphorus-doped CoS_2 as efficient electrocatalyst for hydrogen evolution reaction. Electrochim Acta 259:955–961
2. Liu Z, Xu J, Li Y et al (2018) High performance photocatalytic based on Ce doped $CoWO_4$: controllable synthesis and enhanced photocatalytic activity. Catal Lett 148(10):3205–3213
3. Zou X, Zhang Y et al (2015) Noble metal-free hydrogen evolution catalysts for water splitting. Chem Soc Rev 44(15):5148–5180
4. Xu J, Huo F, Zhao Y et al (2018) In-situ La doped Co_3O_4 as highly efficient photocatalyst for solar hydrogen generation. Int J Hydrog Energy 43(18):8674–8682
5. Liu Y, Yu G, Li GD et al (2015) Coupling Mo_2C with nitrogen-rich nanocarbon leads to efficient hydrogen-evolution electrocatalytic sites. Angew Chem 127(37):10902–10907
6. Meng ZD, Ullah K, Zhu L et al (2014) Modified hydrothermal fabrication of a CoS_2-graphene hybrid with improved photocatalytic performance. Mater Sci Semicond Process 27:173–180
7. Yu H, Xu J, Liu Z et al (2018) Functionalization of sheet structure MoS_2 with CeO_2-Co_3O_4 for efficient photocatalytic hydrogen evolution. J Mater Sci 53(21):15271–15284
8. Li Y, Xu J, Liu Z et al (2018) Performance of amorphous CoS_x/oxygen vacancies ZnO heterojunction photocatalytic hydrogen evolution. J Mater Sci: Mater Electron 30(1):246–258
9. Zhu M, Han M, Zhu C et al (2018) Strong coupling effect at the interface of cobalt phosphate-carbon dots boost photocatalytic water splitting. J Colloid Interface Sci 530:256–263
10. Wang M, Lin M, Li J et al (2017) Metal-organic framework derived carbon-confined Ni_2P nanocrystals supported on graphene for an efficient oxygen evolution reaction. Chem Commun 53(59):8372–8375
11. Zheng S, Li X, Yan B et al (2017) Transition-metal (Fe Co, Ni) based metal-organic frameworks for electrochemical energy storage. Adv Energy Mater 7(18):1602733
12. Dong B, Li W, Huang X et al (2019) Fabrication of hierarchical hollow Mn doped $Ni(OH)_2$ nanostructures with enhanced catalytic activity towards electrochemical oxidation of methanol. Nano Energy 55:37–41
13. Li Q, Chen Y, Yang T et al (2013) Preparation of 3D flower-like NiO hierarchical architectures and their electrochemical properties in lithium-ion batteries. Electrochim Acta 90(5):80–89
14. Chen J, Zheng J et al (2015) A highly sensitive non-enzymatic glucose sensor based on tremella-like $Ni(OH)_2$ and Au nanohybrid films. J Electroanal Chem 749:83–88
15. Liu C, Chen Q, Hao Y et al (2019) $Ni(OH)_2$/$NiSe_2$ hybrid nanosheet arrays for enhanced alkaline hydrogen evolution reaction. Int J Hydrog Energy 44(10):4832–4838
16. Wang T, Pan J, Gasore Achille K et al (2017) A green dual complexation precipitation synthesis of hierarchical α-$Ni(OH)_2$, microspheres and their electrochemical performance. Int J Hydrog Energy 42(30):19139–19147
17. Krehula S, Ristića M, Wu C et al (2018) Influence of Fe(III) doping on the crystal structure and properties of hydrothermally prepared β-$Ni(OH)_2$ nanostructures. J Alloys Compd 750:687–695
18. Zhao J, Zhang Q et al (2015) Synthesis of $Ni(OH)_2$ nanoflakes through a novel ion diffusion method controlled by ion exchange membrane and electrochemical supercapacitive properties. Electrochim Acta 184:47–57
19. Chen X, Chen S, Lin C et al (2015) Nickels/CdS photocatalyst prepared by flowerlike Ni/$Ni(OH)_2$ precursor for efficiently photocatalytic H_2 evolution. Int J Hydrog Energy 40(2):998–1004
20. Jose G, Joseph C, Ittyachen MA et al (2007) Structural and optical characterization of CdSe nanocrystallites/rare earth ions in sol-gel glasses. Opt Mater 29(11):1495–1500
21. Mani KP, George V, Ramakrishnan BP et al (2015) Synthesis and photoluminescence studies of one dimensional Sm_2MoO_6 nanofibers derived from electrospinning process. J Mater Res Technol 4(2):224–227
22. Tao D, Meng L, Peng W et al (2018) Synthesis of hierarchical tube-like yolk-shell Co_3O_4@$NiMoO_4$, for enhanced supercapacitor performance. Int J Hydrog Energy 43(31):14569–14577
23. Du P, Yu JS et al (2017) Near-ultraviolet light induced visible emissions in Er^{3+}-activated La_2MoO_6 nanoparticles for solid-state lighting and non-contact thermometry. Chem Eng J 327:109–119
24. Yu L, Nogami M (2010) The synthesis and photoluminescent properties of one-dimensional $ZnMoO_4$: Eu^{3+} nanocrystals. Mater Lett 64(14):1644–1646
25. Ghorai TK, Dhak D, Biswas SK et al (2007) Photocatalytic oxidation of organic dyes by nano-sized metal molybdate incorporated titanium dioxide ($M_xMo_xTi_{1-x}O_6$) (M = Ni, Cu, Zn) photocatalysts. J Mol Catal A 273(1):224–229
26. Ray SK, Dhakal D, Kshetri YK et al (2017) Cu-α-$NiMoO_4$, photocatalyst for degradation of methylene blue with pathways and antibacterial performance. J Photochem Photobiol, A 348:18–32

27. Namvar F, Beshkar F, Salavati-Niasari M et al (2017) Novel microwave-assisted synthesis of leaf-like $MnMoO_4$ nanostructures and investigation of their photocatalytic performance. J Mater Sci: Mater Electron 28(11):7962–7968
28. Mani Kamal P, Vimal G, Biju PR et al (2015) Optical nonlinearity and photoluminescence studies of red emitting samarium molybdate nanophosphor. ECS J Solid State Sci Technol 4(5):67–71
29. Chen L, Zhang J, Ren X et al (2017) $Ni(OH)_2$-CoS_2 hybrid nanowire array: a superior non-noble-metal catalyst toward the hydrogen evolution reaction in alkaline media. Nanoscale 9(43):16632–16637
30. Yu H, Xu J, Guo H et al (2017) Synergistic effect of rare earth metal Sm oxides and $Co_{1-x}S$ on sheet structure MoS_2 for photocatalytic hydrogen evolution. RSC Adv 7(89):56417–56425
31. Huang Y, Cui F, Zhao Y et al (2018) $NiMoO_4$ nanorod deposited carbon sponges with ant-nest-like interior channels for high-performance pseudocapacitors. Inorg Chem Front 5(7):1594–1601

Affiliations

Zeying Liu[1] · Jing Xu[1,2,3] · Qiuting Liao[1] · Yanru Li[1] · Lingjiao Li[1] · Min Mao[1]

[1] School of Chemistry and Chemical Engineering, North Minzu University, Yinchuan 750021, People's Republic of China

[2] Key Laboratory of Chemical Engineering and Technology (North Minzu University), State Ethnic Affairs Commission, Yinchuan 750021, People's Republic of China

[3] Ningxia Key Laboratory of Solar Chemical Conversion Technology, North Minzu University, Yinchuan 750021, People's Republic of China